

This is a revised version of an article submitted for consideration in Ultramicroscopy (copyright Elsevier). Ultramicroscopy is available online at:  
<http://www.journals.elsevier.com/ultramicroscopy/>

## **Orientation precision of TEM-based orientation mapping techniques**

A.Morawiec<sup>1</sup>, E.Bouzy<sup>2</sup>, H.Paul<sup>1</sup>, J.J. Funderberger<sup>2</sup>,

<sup>1</sup> Institute of Metallurgy and Materials Science, Polish Academy of Sciences,  
Kraków, Poland.

<sup>2</sup> Laboratoire d'Etude des Microstructures et de Mécanique des Matériaux,  
Université de Metz, Metz, France

E-mail: nmmorawi@cyf-kr.edu.pl, Tel.: ++48-122952854, Fax: ++48-122952804

---

### **Abstract**

Automatic orientation mapping is an important addition to standard capabilities of conventional transmission electron microscopy (TEM) as it facilitates investigation of crystalline materials. A number of different such mapping systems have been implemented. One of their crucial characteristics is the orientation resolution. The precision in determination of orientations and misorientations reached in practice by TEM-based automatic mapping systems is the main subject of the paper. The analysis is focused on two methods: first, using spot diffraction patterns and 'template matching', and second, using Kikuchi patterns and detection of reflections. In simple terms, for typical mapping conditions, their precisions in orientation determination with the confidence of 95% are, respectively, 1.1° and 0.3°. The results are illustrated by example maps of cellular structure in deformed Al, the case for which high orientation sensitivity matters. For more direct comparison, a novel approach to mapping is used: the same patterns are solved by each of the two methods. Proceeding from a classification of the mapping systems, the obtained results may serve as indicators of precisions of other TEM-based orientation mapping methods. The findings are of significance for selection of methods adequate to investigated materials.

---

**Keywords:** Transmission electron microscopy; Electron diffraction; Orientation mapping; Misorientation; Indexing; Aluminum

## 1. Introduction

The technique of orientation mapping based on transmission electron microscopy (TEM) is in many respects similar to the mapping by scanning electron microscopy (SEM) and electron backscattered diffraction (EBSD) widely applied to investigation of microstructures and textures of polycrystalline materials. Systems of both types use electron diffraction to determine local orientations of crystallites, and both provide digital maps with orientation parameters ascribed to individual pixels of the maps. The TEM-based mappings have a narrower scope of applications, are less convenient and, consequently, less popular than EBSD. There is, however, a considerable variety of TEM-based mapping systems with significant differences between them, and there is a steady flow of ideas for advancing the technique. These systems have been created primarily as extra tools for TEM microscopists. In some cases, the goal was not only the mapping, but also an easy access to orientations of individual crystallites (as getting an orientation by a click of a button is more convenient than a tedious search for recognizable zone axes). The other objectives were potential applications to cases inaccessible by EBSD systems.

For applications complementary to those of EBSD, two aspects of TEM-based orientation determination are of particular importance: the spatial resolution and the resolution in the orientation space, i.e., the sensitivity to crystal orientation. A number of different claims concerning the latter issue can be encountered in literature. Usually, an orientation determination method is characterized by just one parameter – an all-embracing ”angular resolution”. This leads to confusion because with such an approach, one fails to discriminate, first, between precision (repeatability, linked to random errors) and accuracy (closeness to true values, linked to systematic errors), second, between resolutions for orientations and misorientations, and third, between a careful interactive (mis)orientation measurement and automatic mappings. Moreover, a single ”angular resolution” is insufficient when the errors are different for different orientation parameters.

The orientation resolution in automatically acquired TEM-based maps is the main subject of this paper. At the background, a general description of the capabilities of TEM-based mapping systems will be given. Since a number of different approaches have been implemented, they are classified based on the type of utilized patterns, methods of acquiring the patterns, and methods of solving them. Then, particular implementations are briefly described. Subsequent sections concern (mis)orientation resolution of particular methods and reliabilities of automatically obtained orientations. Conclusions on orientation resolution are drawn from analysis of both small sets of diffraction patterns (with a better control

of particular steps) and large automatically treated sets. The opportunity is taken to introduce a combined approach in which the same experimental patterns are solved by two different methods: as spot patterns and as Kikuchi patterns. Before closing remarks, the scope of misindexing linked to '180° ambiguity' is considered. Although the paper derives from experience of both creators and users of one of the systems, no particular mapping method is promoted, and all existing techniques designed for medium-voltage (primarily 200kV) transmission microscopes are taken into consideration.

## 2. Methods of mapping

There are a variety of ways to determine crystal orientations using TEM. Small sets of orientations can be obtained by manual detection of positions of diffraction reflections, and there are numerous programs for computer-assisted analysis of TEM diffraction patterns (e.g., [1,2]). However, such interactive approaches are not suitable for orientation mapping. The mappings require some automation because thousands of patterns need to be solved. Thus, at least the acquisition of the patterns and calculation of orientations at individual points of a map must be carried out automatically.

Both basic types of electron diffraction patterns, spot patterns and line patterns, can be used for orientation determination. However, of various forms of these patterns only some are applicable to mapping; the standard selected area diffraction (with parallel electron beam and the diffracting area selected by an aperture at the image plane of the objective lens) and the 'defocused' methods (of displaying the image on top of the diffraction pattern) are not suitable for mapping because of their poor spatial resolution [3]. On the other hand, with focused-probe techniques, when the electron beam converges on the specimen, the size of the electron probe can be very small, and the spatial resolution is appropriate for mappings. By increasing the beam convergence angle, a diffraction pattern changes from a nano-beam diffraction pattern when the half-angle is much smaller than the Bragg angle, through a Kossel–Möllenstedt pattern composed of non-overlapping disks, to a Kossel pattern composed of overlapping disks when the half-angle is larger than the Bragg angle. With a large convergence angle, deficiency and excess lines are visible inside the disks. The geometry of the lines is the same as in Kikuchi patterns resulting from diffraction of divergent diffusely scattered electrons and thus observable for sufficiently thick specimens. Out of the focused-probe diffraction methods, those with small convergence angle and those generating patterns with Kikuchi component have been used for automatic orientation mappings.

Some diffraction techniques can be combined with the rocking beam mode in which

the incident beam is tilted and rotated around the optical axis of the microscope. Under computer control, diffraction patterns or dark field images can be recorded at particular beam positions. The positions and the patterns or images are used for further processing and orientation determination. Acquisition of nano-beam diffraction spot patterns can be augmented by precession electron diffraction (PED) [4]. In PED, the incident beam and the transmitted beam are moved in a coordinated manner so the obtained patterns look like spot patterns but more spots are observed, and the solid angle covered by the diffraction spots is increased. PED patterns are also claimed to be "less dynamical" than classical spot patterns, i.e., intensities on experimental PED patterns are closer to the kinematic approximation. As in the original technique [4], the beam can be controlled by extra hardware, but there exists an alternative method utilizing built-in microscope capabilities and additional software for controlling the beams [5]. The latter approach is yet to be applied for orientation mapping.

Let us note that orientation maps are also obtained by *transmission* Kikuchi diffraction in SEM, e.g., [6]. This technique differs from TEM-based Kikuchi diffraction in two important respects: the electron energy and the specimen-to-detector distance (acceptance angle), and as such, it is outside the scope of this paper.

#### *Map acquisition*

There are currently two main methods of acquisition of TEM-based orientation maps:

- acquisition of dark-field microstructure images at various incident beam directions (for brevity, we will refer to this method as **A**); parameters of directions at which a pixel of the image gets bright are used to calculate the orientation corresponding to this pixel,
- stepwise scanning of the specimen by the electron beam and acquisition of a diffraction pattern at each step of the scan (**B**).

The acquisition methods of type **A** imply the use of spot patterns [7]. One can devise an **A**-type approach, in which orientation is calculated without explicitly constructing diffraction patterns, but the procedure will still be computationally equivalent to solving spot patterns as long as it uses the directions of the incident beam and locations of brightened pixels (equivalent to the directions of diffracted beams).

In orientation mappings, diffraction patterns or microstructure images are recorded with internal (in-column) TEM cameras or using external video cameras. Digital cameras with high dynamic ranges, e.g., slow-scan CCD cameras, allow for considerable pattern enhancements. Such enhancements are crucial for solving some patterns; in particular, image processing may lead to significant improvement in the quality of Kikuchi patterns (Fig. 1). On the other hand, when applied to the stepwise scanning (**B**), slow-scan cameras have the

Fig. 1

disadvantage of long times of map acquisition.

Some authors argue that the procedures of type B are unreliable because of a drift of the beam with respect of the specimen [7]. It must be noted at the outset that our experience (with CM20 and CM200 Philips microscopes) does not confirm these concerns. Large drifts would visibly distort the maps, and no such effects were observed. Moreover, post-mapping examinations of contamination spots reveal no visible drift for acquisition times as long as eight hours.

#### *Calculation of crystal orientation*

There are two main approaches to orientation determination from the diffraction patterns. It is carried out via either

- grid search in orientation space (a) or
- detection of positions of individual reflections and their indexing (b).

The brute-force grid search in orientation space (a) is widely used in various areas of crystallography, e.g., [8]; it is applied in combination with "template matching" to solve (spot) diffraction patterns [9]. Briefly, orientations are determined by matching experimental patterns to simulated patterns (templates) pre-calculated for a grid in the orientation space. The matching can be based on geometry alone (binary patterns) or may also involve intensities in the patterns. The orientation corresponding to the template with the best match is taken as the crystallite orientation. The density of the grid and crystal symmetry determine the number of templates. The density is directly linked to the orientation sensitivity of the diffraction patterns; with the relatively low sensitivity of spot patterns, the number of templates can be reasonably small. On the other hand, the grid search in orientation space is not suitable for solving patterns highly sensitive to orientation when a prohibitive number of templates would be required.

All types of diffraction patterns (including orientation-sensitive patterns) can be solved by detecting positions of reflections and subsequent analysis of their geometry, i.e., via the approach b. Appropriate software detects features specific to given patterns: peaks with certain characteristics in spot patterns, and lines in Kikuchi patterns. (In the latter case, the detection of lines is standardly carried out by searching for peaks in the Hough transform of the pattern.) It needs to be stressed that diffraction patterns of the same type may exhibit considerable diversity. Their contrast, brightness, sharpness of reflections, complexity of the geometry of reflections depend on structure of the investigated material, its state, and operating conditions of the microscope. Thus, maximum flexibility is desired so the detection is applicable to a wide range of materials and microscope settings. This

flexibility is one of the crucial factors determining the quality of a procedure for detection of reflections. With known locations of reflections, their geometry is then used to index the pattern, i.e., to assign Miller indices to each legitimate reflection.

In the case of diffraction patterns originating from known structures, orientation determination is practically equivalent to indexing. Clearly, based on crystal orientation, the locations and indices of reflections can be obtained, and the opposite is also true: knowing Miller indices and exact locations of reflections, one can easily calculate the orientation. However, due to the discreteness of Miller indices, the indexing has dichotomous character: it is either correct or incorrect. On the other hand, even with correct indexing, experimentally determined continuous orientation parameters (e.g., rotation axis  $\mathbf{n}$  and angle  $\omega$ ) are afflicted by errors, i.e., a measured orientation differs slightly from the true orientation.

### *Implementations*

The first TEM-based orientation mapping system (usually referred to as "conical dark field scanning") introduced by Wright and Dingley [10] uses **A**-type acquisition, "reconstructed" spot-type patterns and **b**-type indexing based on detection of reflections [7,11]. Also a version of the "conical dark field scanning" with the grid search for orientations (i.e., of type **a**) has been put together [12]. Moreover, a three-dimensional (3D) variant of the "conical dark field scanning" has been recently described [13]. For getting a 3D map, conical dark-field images were recorded for many tilts of the specimen, and orientations for individual voxels (volume elements) were determined by analysis of intensities on the images over all beam directions and sample tilt positions. The indexing, described by authors as "reduced grid search" [14] uses the idea of accumulating intensities of reflections in feasible bins into which the orientation space is divided [15].

Maps are also created using the nano-beam diffraction spot patterns and the stepwise scanning of the specimen (**B**) combined with the grid search in orientation space (**a**) [9] or detection of reflections (**b**) [16]. To reduce indexing ambiguities (see below), the former approach has been coupled with PED [17].

Finally, there exists a mapping system based on transmission Kikuchi patterns [18,19]<sup>1</sup>. By the character of the patterns, it is of type **B** & **b**, i.e., the stepwise scanning is combined with indexing by finding locations of Kikuchi lines.

Summarizing, the existing orientation mapping systems use all the combinations **A** & **a**, **A** & **b**, **B** & **a** and **B** & **b** with spot patterns, and **B** & **b** with Kikuchi patterns (Table 1). Our

Tab. 1

---

<sup>1</sup>A similar system has been announced earlier [20] but no automatically recorded maps have been published.

focus below will be on two representative cases: spot-based B & a and Kikuchi-based B & b orientation determination.

### 3. Orientation and misorientation resolutions

Accuracy in determination of crystallite orientations in a sample is mainly affected by sample preparation and positioning of the sample in a holder, and it depends very much on skills of an experimenter. Additional errors are caused by bending of thin foils and by misalignments of the microscope (resulting in migration of the pattern center during scanning). The inaccuracies caused by the mapping systems are small compared to the sample positioning errors. Therefore, here, the accuracy of orientations will not be discussed any further; the focus will be on the orientation precision.

The distinction between accuracy and precision of *mis*orientation determination is less straightforward. As sample positioning affects all orientations in the same way, it has no impact on misorientations. In mappings involving diverse orientations, the main systematic contribution to the errors is that caused by foil bending. Moreover, in an automatic measurement of misorientations between two particular crystallites, orientations for a given grain originate from almost identical patterns and are likely to be biased in the same way, i.e., systematic errors arise, and the misorientation accuracy is affected. If these cases are excluded, it is reasonable to assume that the accuracy of misorientations across a grain boundary is determined by their precision, or in other words, that misorientations are affected only by random errors.

Formally, the spread of random (mis)orientation errors should be modeled by a suitable distribution on the rotation space (e.g., von Mises-Fisher distribution). Since the considered errors are small, the corresponding rotations are close to the identity. In the parameterization by the rotation vector  $(\omega_x, \omega_y, \omega_z)$  defined as the unit vector  $\mathbf{n}$  along the rotation axis scaled by the rotation angle  $\omega$ , i.e.,  $(\omega_x, \omega_y, \omega_z) = \omega \mathbf{n}$ , the metric tensor of the rotation space in the neighborhood of the identity is nearly Cartesian. Therefore, it is reasonable to approximate the distributions of random errors by trivariate Gaussian distribution of rotations parametrized by  $(\omega_x, \omega_y, \omega_z)$ . Such distributions of random errors will be further assumed, and precisions will be quantified by standard deviations.

Since an orientation and a misorientation differ by the reference coordinate systems (system of the specimen and system of another crystallite, respectively), and obtaining a misorientation involves two orientation measurements, the standard deviation  $\sigma_m$  of the distribution of misorientation errors is related to the standard deviation  $\sigma_o$  of the distribu-

tion of random orientation errors. With complications related to 'anisotropy' of the errors ignored, one has

$$\sigma_m = \sqrt{2}\sigma_o . \quad (1)$$

In other words, the imprecision in misorientation determination is  $\sqrt{2}$  times larger than the imprecision in orientation determination.

Some of our considerations require the solid angle covered by diffraction patterns. This angle is directly linked to the ratio of camera length  $L$  and pattern diameter  $2r_p$ . It can be conveniently quantified by the acceptance angle  $\xi = 2 \arctan(r_p/L)$ . In the case of dark field imaging (type A methods), the acceptance angle is determined by the angle of beam rocking. Similarly, with PED, the acceptance angle is increased by the precession angle.

In what follows, we describe a number of tests for assessing the orientation and misorientation uncertainties. The first three tests were carried out on small number of patterns with manual emulation of mapping conditions, and the last one, described in the next section, involved only automatically analyzed data.

*Test 1: orientation precision in Kikuchi-based maps*

Kikuchi patterns exhibit relatively high sensitivity to crystal rotations. Various figures have been given as its quantitative descriptors. A careful analysis shows that simple characterization of the Kikuchi-based orientation precision by a single number does not reflect the reality. It was first noted in [21] that the precision of the orientations is much lower than the precision in determination of the direct beam direction. The same observation was more specifically described in [22]: the precision in determination of crystal rotations about the optical axis (referred to as 'z') is much lower than that for rotations about axes perpendicular to 'z'. The former depends mainly on the (fixed) size of the detector, and the latter is determined by the (adjustable) camera length; the larger the camera length, the higher the precision of the rotations about axes perpendicular to 'z'. Both types of rotations are influenced by the diffuseness of Kikuchi lines.

Since the sizes of detectors and the ranges of camera lengths admissible for Kikuchi-based mappings are limited (see below), the precisions can be estimated for settings used in practice. For this purpose, six pairs of lines were marked manually in each of five randomly selected patterns of Ti- $\alpha$ , and this was repeated ten times. The patterns were also solved automatically. Fig. 2a shows the spread of obtained orientations. The standard deviation for the data of Fig. 2a was nearly  $0.12^\circ$  for rotations about the optical axis, and it was about  $0.04^\circ$  for rotations about axes perpendicular to 'z'.

Fig. 2

The patterns had dimensions  $512 \times 512$  pixels. One pixel at the distance of 512 pixels

covers an arc of about  $0.1^\circ$  – the angle slightly smaller than one standard deviation for rotations about 'z'. The precision of these rotations is affected more by the diffuseness of lines and distortions than the pixel size, and therefore, increasing the resolution beyond 512 pixels will not significantly improve this precision. In mapping, the size of the pattern in pixels is directly linked to the efficiency of Hough transform, and it must be reasonably small because the time of pattern processing grows quadratically with the size. For completeness, let us note that the impact of geometric curvature of lines is negligible. The maximal curvature of Kikuchi lines corresponding to reciprocal lattice vectors perpendicular to the optical axis is  $\tan\theta/L$ , where  $\theta$  is the Bragg angle. For the considered voltages and camera lengths the curvatures are small, and with the small acceptance angle, the lines can be treated as straight.

Fig. 2a needs to be compared to Fig. 2b obtained (from patterns of Si) with a much larger camera length; they show similar spreads of rotations about the optical axis, but the spread of rotations about axes perpendicular to 'z' is much smaller in Fig. 2b than in 2a. The high precision for beam direction led to claims that the "accuracy" of orientations determined from Kikuchi patterns "can be as high as approximately  $0.01^\circ$ " [23]. This number could be a rough estimation of the precision of rotations about axes perpendicular to 'z' for patterns recorded with large camera lengths, not suitable for indexing because of small acceptance angle.

Summarizing, with typical limitations on the acceptance angle and typical diffuseness of Kikuchi lines, the orientations in Kikuchi-based maps are expected to have precisions similar to that of the data shown in Fig. 2a. In 'manual' analysis of individual patterns, the precision of rotations about axes perpendicular to the optical axis can be easily increased by increasing the camera length, but to improve the precision of the rotation about the optical axis, more complex procedures are necessary [22].

*Test 2: accuracy of misorientations in Kikuchi-based maps*

To estimate the accuracy of misorientations in maps, one needs to refer experimental results to true misorientations. The coherent recrystallization twins easily discernible in maps of face centered cubic (A1) metals have the definite  $\Sigma 3$  misorientation. Therefore, they are a convenient case for testing the accuracy of misorientation determination.

An example distribution of deviations of fifty measured misorientations between coherent twins from the ideal  $\Sigma 3$  misorientation is shown in Fig. 3. The data originate from three maps of specimens recrystallized after deformation of  $(112)(111)$  oriented single crystals of: Cu and Cu-2%wtAl, both partly recrystallized (60s at 460C) after 50% channel-die

Fig. 3

deformation, and Ag recrystallized (30s at 265C) after 67% deformation. The deviation of the mean [24] of the measured misorientations from the ideal  $\Sigma 3$  was  $0.13^\circ$ , and the standard deviation from the mean was within  $0.20 - 0.28^\circ$  for each of the parameters  $\omega_x, \omega_y, \omega_z$ . This standard deviation is consistent with the above obtained (Test 1) standard deviation for orientations and eq.(1).

For comparison, it is worth noting that for analogous data obtained from one of our EBSD-based maps (Cu specimen partly recrystallized (60s at 460C) after 50% channel-die deformation of (112) $\langle$ 111 $\rangle$  oriented single crystal), the deviation of the mean misorientation from the ideal  $\Sigma 3$  was  $0.50^\circ$ , and the standard deviation from the mean was nearly  $0.40^\circ$ ; see also [25].

*Test 3: orientation precision in spot-based maps*

Since spot patterns are relatively insensitive to crystal orientation, the precision of orientations determined from such patterns must be limited. The imprecision is associated with the excitation error due to the thinness of the specimen; e.g., [3]. It is easy to see that the excitation error has an effect only on the precision of beam direction. The error of rotation about the optical axis is determined by the size of the pattern detector and sizes of the spots. With the grid search approach (a), the precision of orientation is linked to the density of the grid, i.e., to the number of templates.

The orientation precision in the spot-based mapping can be estimated using spot patterns in which also Kikuchi lines are visible. The imprecision in beam direction obtained from spot patterns is expected to be considerably larger than that from Kikuchi patterns, and one can assume that the latter is negligible. To characterize quantitatively the orientation precision for spot-based maps, example fifty patterns of Al were picked from a set collected for a map (Fig. 4a); the choice was random except the condition that Kikuchi lines were visible sufficiently well. The patterns were solved manually using the Kikuchi lines and automatically using the spots (based only on spot locations, i.e., without fitting intensities), and deviations between such obtained orientations were calculated. The cumulative distributions of the deviations for various template densities are shown in Fig. 4b; in its legend and below, the number of templates is given in the form: (the number of different beam directions  $\times$  the number of rotations about the optical axis). For the smallest number of templates ( $254 \times 120$ ), the deviations are larger than for the remaining three sets; the latter do not differ much between themselves. This demonstrates that for the Al structure, increasing the number of templates beyond  $\sim 1000$  beam directions does not lead to any considerable improvement. For the limiting number of templates ( $976 \times 240$ ), the grid step

Fig. 4

is approximately  $1.6^\circ$  for the beam direction, and it is  $360^\circ/240 = 1.5^\circ$  for the rotations about 'z'. The distribution of deviations between Kikuchi- and spot-based orientations for the largest number of templates ( $5975 \times 600$ ) is shown Fig. 4c. The standard deviation of the rotations about axes perpendicular to 'z' was  $\sim 0.53^\circ$ . As for the rotation about the optical axis, the standard deviation was similar ( $0.52^\circ$ ), but this value is affected by lower precision of the reference Kikuchi-based data for this axis.

After completing the initial grid search, one can additionally refine the orientation by a local search for orientations with better matching templates. In the implementation described in [9] and also in our software [26], the templates are pre-calculated for a grid of beam directions, and a single template is used for examining all orientations differing by a rotation about the optical axis of the microscope. Having stored only the templates for a grid of beam directions, the refinement of the rotation about  $z$  is simpler than refining the other two orientation parameters because it does not require any extra templates.

#### *Precisions of other spot-based approaches*

In the context of orientation sensitivity, the variant of spot-based mapping with precession needs to be commented on. The PED technique is equivalent to a stationary beam and precession of the specimen. Thus, the solid angle covered by the diffraction spots is increased at the cost of increasing the range of orientations responsible for a PED pattern. The larger the precession angle, the larger the range, and consequently, the lower the orientation resolution. In effect, this approach does not improve the orientation precision.

As for the precision of orientations determined by spot detection methods (b), one may expect it to be similar to that of "template matching" with a search through a dense grid (a). The reports [7,16] indicate that, in practice, reaching such precision with spot detection methods turns out to be difficult. In the case of conical dark field, the estimation of precision depends strongly on the quality of diffraction patterns reconstructed from dark-field images.

Finally, in 3D mapping, multiple diffraction patterns acquired at various tilt angles contribute to resulting orientations. This clearly creates a potential for increasing the precision of (mis)orientations. Its quantitative measure is yet to be determined.

The findings of this section are briefly summarized in Table 2. It contains explicit values of two standard deviations corresponding to the confidence of 0.95 which is considered to be most suitable for the quantification of the orientation precision. These results were obtained using just one particular implementation, but they are believed to be reasonable estimates and may serve as reference data.

Tab. 2

#### 4. Impact of orientation precision on maps – an example

How do the differences in precision influence orientation maps? To illustrate the effect, we selected the cellular structure in deformed aluminum, i.e., one of the cases for which the orientation resolution does play a role. The specimen was severely deformed by ECAP. The induced microstructure consists of bands with only slightly misoriented cells inside the bands (Fig. 5). Knowing the level of misorientations between the bands and inside the bands (between cells), and the size of the cells is crucial for understanding the process of grain subdivisions during severe plastic deformation. Since the investigated misorientations are small, they are properly depicted in maps only when the mapping system is sufficiently sensitive to orientation changes.

Fig. 5

Kikuchi and spot diffraction patterns (Fig. 6a and b) were collected with 20nm steps from approximately the same areas. We used Philips CM200 microscope operating at the nominal voltage of 200kV and equipped with Gatan 791 slow-scan CCD camera and software for automatic pattern acquisition [19]. The Kikuchi patterns were recorded in nano-probe mode with the probe size of 5nm and the acceptance angle  $\xi = 16.8^\circ$ . The spot patterns were recorded in micro-probe mode with the probe size of 20nm and the acceptance angle of  $9.0^\circ$ . The diffraction patterns were then indexed using the software described in [18] and [26].

Fig. 6

Since the mapping areas, tilt angles and probe sizes in the two mappings were slightly different, we additionally processed the spot patterns to enhance the weak Kikuchi components, and to get a Kikuchi-based map from exactly the same area as the spot-based map. The Kikuchi lines were amplified by application of high-pass filter and subsequent contrast enhancement. The resulting patterns (Fig. 6c) had different characteristics from those originally recorded as Kikuchi patterns (Fig. 6a) and the line detecting software required slightly different input parameters, but besides that, the indexing process was the same. For the orientations present in the material, the difference in camera length had no impact on the reliability of indexing.

The three orientation maps are shown in Fig. 7. Orientations ascribed to pixels differ between themselves only slightly. In all cases, the beam direction is close to  $\langle 215 \rangle$ . The maps illustrate the impact of the orientation precision: the cellular character of the structure is clearly visible in Kikuchi-based maps, and it is blurred in the spot-based map. This is confirmed by misorientation profiles (Fig. 8). The profiles obtained from Kikuchi patterns contain plateaus corresponding to stable orientations of cell interiors, whereas the profiles obtained from spot patterns are much more jerky. The map of angular distances between spot-based and Kikuchi-based orientations and the cumulative distribution of these distances

Fig. 7

Fig. 8

are shown in Fig. 9. More than 97% of orientations differ by less than  $5^\circ$ , and the remaining 3% correspond to 'spikes' and 'no solution' pixels of the map shown in Fig. 7c. With the outliers exceeding  $5^\circ$  excluded, the average angular distance is  $0.83^\circ$ . The distribution of the distances shown in Fig. 9b matches those of Fig. 4b for dense orientation grids. Fig. 9

## 5. Misindexing

The precision is just an aspect of the more general issue of reliability of orientations in maps. Most difficulties with the reliability are sample-specific. Crystal defects, strain gradients, grain boundaries, multiple-grain contributions decrease the quality of diffraction patterns. In methods of type **b**, poor quality of patterns makes line or spot detection difficult, and in consequence, it may lead to incorrect orientations. Similarly, with "template matching" (**a**), there is an increased probability of ascribing a wrong template and ultimately an incorrect orientation. Robustness to pattern imperfections is a crucial feature of the orientation mapping systems.

However, there is also an issue of instrumental character: it is the notorious "180° orientation ambiguity", e.g., [27]. This problem is usually attributed to spot patterns [23], but it equally affects Kikuchi patterns. In geometry-based indexing, it arises when the reciprocal space vectors corresponding to reflections used for solving a pattern are coplanar. In practice, this means that the solid angle covered by a diffraction pattern is insufficiently large. A narrow-angle spot pattern may contain reflections of just one (zeroth-order) Laue zone. This is likely to occur when the spots of the first-order Laue zone are missing due to systematic extinctions [26]. Unless the zone axis happens to be a two-fold symmetry axis, such patterns correspond to two non-equivalent orientations (Fig. 10a). Similarly, Kikuchi patterns with detectable lines belonging to just one zone axis give ambiguous solutions (Fig. 10b). For the A1 and A2 structures, the most susceptible to the "180° ambiguity" are the orientations with incident beam directions close to  $\langle 112 \rangle$  and  $\langle 111 \rangle$ , respectively.<sup>2</sup> Fig. 10

In principle, the "180° ambiguity" can be resolved by increasing the acceptance angle, but there are factors severely limiting such increases. One of them is the deterioration of diffraction patterns at large scattering angles. In spot patterns, the acceptance angle equals four times the largest of Bragg angles of reflections used for solving the pattern. For simple cubic structures and the voltage of 200kV,  $\xi$  is typically about  $7^\circ$ . The increase of the acceptance angle to avoid the indexing ambiguities is one of the reasons for using PED in B-type acquisition of spot patterns [17]. The use of precession alleviates the problem but

---

<sup>2</sup>It is worth noting that also EBSD  $\langle 111 \rangle$  zone axis patterns of A1 structures are affected by the "180° ambiguity"; see [28] and references therein.

it does not resolve it completely because in extreme cases, like the  $\langle 111 \rangle$  zone axis of A2 structures, very large precession angles would be needed to ascertain the right solutions; on the other hand, the angles must be kept small (tenths of a degree) in order to retain a higher precision in orientation determination.

Image processing applied to Kikuchi patterns considerably enhances the intensities at large scattering angles, but the acceptance angle is limited by instruments; with large angles (i.e., small camera lengths), shadows of apertures appear in the patterns. For the Gatan 791 slow-scan CCD camera installed on CM200, the largest acceptance angle not leading to such shadows is  $\xi \approx 17.0^\circ$ . The Gatan DV300W camera on CM20 microscope gives at most the angle  $\xi$  of  $13.4^\circ$ . To guarantee solvability of all patterns, the acceptance angle should be larger than a limit depending not only on the crystal structure but also on the robustness of the line detection and quality of the patterns.

The other way of limiting misindexing is to have orientations determined at various specimen tilts. Recording of patterns at multiple tilts is an integral part of the three-dimensional mapping described in [13]. The reliability of this approach in automatic mode is yet to be determined.

## 6. Final remarks

The obtained results confirm that the precision of orientations obtained from Kikuchi patterns is 'anisotropic', i.e., different for different axes. With microscope settings typical for orientation mappings, the standard deviation for rotations about axes perpendicular to the optical axis 'z' was found to be three times smaller than standard deviations for rotations about 'z'. For spot patterns, the distribution of random orientation errors was found to be close to isotropic. With the confidence of 95%, the orientation (misorientation) data on maps obtained from geometry of spot patterns are within  $1.1^\circ$  ( $1.5^\circ$ ) from mean results. Disregarding the anisotropy, with the same confidence of 95%, the orientation (misorientation) data on Kikuchi-based maps are within  $0.3^\circ$  ( $0.4^\circ$ ) from mean results. (The latter precision is higher than that of SEM-EBSD data roughly by the factor of two.) Due to small acceptance angles of TEM diffraction patterns, maps acquired at one specimen tilt can be affected by  $180^\circ$  orientation ambiguity, and this concerns both spot and Kikuchi patterns.

Particular TEM-based orientation mapping systems differ in various respects. This paper was focused on the resolution in orientation space, but there are also differences in spatial resolution, robustness to crystal defects, acquisition times, et cetera. From the viewpoint of a TEM user, the best solution would be to have a larger system with combined

capabilities. Mixing different approaches is partly limited by hardware, but some combinations are definitively possible and they will certainly appear in the future. The use of both spot patterns and Kikuchi patterns demonstrated in this study is an advance toward such systems. In particular, the mapping based on combination of spot and Kikuchi components of the same patterns is a step toward more comprehensive exploitation of information contained in diffraction data. Clearly, not all spot patterns have sufficiently strong Kikuchi component, but this aspect can be controlled by choosing properly thick area of the foil. If applicable, the method may be useful for further improvements in precision and reliability of orientations.

There is a question whether it is worth investing in further development of TEM-based orientation mapping systems when EBSD has comparable (orientation and spatial) resolutions, and a much higher efficiency in terms of the time needed for sample preparation and mapping [23]. Clearly, the scope of applications of TEM differs from that of SEM. In some studies, the same specimen is investigated by both SEM (to get orientations) and TEM (to get other characteristics); see, e.g. [29], . It is, however, much more convenient to determine the orientations directly by TEM. In other words, no matter what are the capabilities of particular systems, TEM needs to be autonomous in respect of orientation determination. To put it bluntly, a scanning microscope with EBSD may be an absolutely better instrument for orientation determination, but it will not provide orientations for a specimen inserted into a transmission microscope. Therefore, the advance of TEM-based orientation determination systems is to some extent independent of the progress in SEM-based systems. An analytical transmission microscope is a versatile instrument with various imaging modes and relatively broad analytical capabilities, and an easy access to crystal orientation is definitely of importance for a complete characterization of crystalline materials investigated by TEM.

### **Acknowledgments**

The authors are grateful to K.Glowinski for his comments on the manuscript. This work was supported in part by National Science Centre (Poland) under grant number N507 301040.

## References

- [1] D. Belletti, G. Calestani, M. Gemmi, A. Migliori, QED V 1.0: a software package for quantitative electron diffraction data treatment, *Ultramicroscopy* **81** (2000) 57–65.
- [2] L. Jiang, D. Georgieva, J.P. Abrahams, EDIFF: a program for automated unit-cell determination and indexing of electron diffraction data *J. Appl. Cryst.* **44** (2011) 1132–1136.
- [3] D.B. Williams, C.B. Carter, *Transmission Electron Microscopy: A Textbook for Materials Science*, Springer, New York, 2009.
- [4] R. Vincent, P. Midgley, Double conical beam-rocking system for measurement of integrated electron diffraction intensities, *Ultramicroscopy* **53** (1994) 271–282.
- [5] C.T. Koch, Aberration-compensated large-angle rocking-beam electron diffraction *Ultramicroscopy* **111** (2011) 828–840.
- [6] N. Brodusch, H. Demers, R. Gauvin, Nanometres-resolution Kikuchi patterns from materials science specimens with transmission electron forward scatter diffraction in the scanning electron microscope, *J. Microsc.* **250** (2013) 1–14.
- [7] D.J. Dingley, Orientation imaging microscopy for the transmission electron microscope, *Microchim. Acta* **155** (2006) 19–29.
- [8] E.E. Lattman, Optimal sampling of the rotation function, *Acta Cryst.* **B28** (1972) 1065–1068.
- [9] E.F. Rauch, L. Dupuy, Rapid diffraction patterns identification through template matching, *Arch. Metall. Mater.* **50** (2005) 87–99.
- [10] S.I. Wright, D.J. Dingley, Orientation imaging in the transmission electron microscope, *Mater. Sci. Forum* **273–275** (1998) 209–214.
- [11] D.J. Dingley, M.M. Nowell, The use of electron backscatter diffraction for the investigation of nano crystalline materials and the move towards orientation imaging in the TEM, *Microchim. Acta* **147** (2004) 157–165.
- [12] G. Wu, S. Zaefferer, Advances in TEM orientation microscopy by combination of dark-field conical scanning and improved image matching, *Ultramicroscopy* **109** (2009) 1317–1325.

- [13] H.H. Liu, S. Schmidt, H.F. Poulsen, A. Godfrey, Z.Q. Liu, J.A. Sharon, X. Huang, Three-dimensional orientation mapping in the transmission electron microscope, *Science* **332** (2011) 833–834.
- [14] S. Schmidt, Private communication.
- [15] A.Morawiec, M.Bieda, On algorithms for indexing of K-line diffraction patterns, *Arch. Metall. Mater.* **50** (2005) 47–56.
- [16] V. Kumar, Orientation imaging microscopy with optimized convergence angle using CBED patterns in TEMs, *IEEE Trans. Image Process.* (2013) to appear.
- [17] E.F. Rauch, M. Véron, J. Portillo, D. Bultreys, Y. Maniette, S. Nicolopoulos, Automatic crystal orientation and phase mapping in TEM by precession diffraction, *Microscopy and Analysis* **22** (2008) S5–S8.
- [18] A. Morawiec, J.J. Fundenberger, E. Bouzy, J.S. Lecomte, EP – a program for orientation determination from Kikuchi and CBED patterns, *J. Appl. Cryst.* **35** (2002) 287.
- [19] J.J. Fundenberger, A. Morawiec, E. Bouzy, J.S. Lecomte, Polycrystal orientation maps from TEM, *Ultramicroscopy* **96** (2003) 127–137.
- [20] R.A. Schwarzer, J. Sukkau, Automated crystal orientation mapping (ACOM) with a computer-controlled TEM by interpreting transmission Kikuchi patterns. *Mater. Sci. Forum* **273-275** (1998) 215–222.
- [21] V.Y. Gertsman, A.P. Zhilyaev, Accuracy in determining grain disorientation in the electron microscope, *Zavod. Lab.* **56** (1990) 30–34.
- [22] A. Morawiec, A method of precise misorientation determination, *J. Appl. Cryst.* **36** (2003) 1319–1323.
- [23] S. Zaefferer, A critical review of orientation microscopy in SEM and TEM, *Cryst. Res. Technol.* **46** (2011) 607–628.
- [24] A. Morawiec, A note on mean orientation, *J. Appl. Cryst.* **31** (1998) 818–819.
- [25] S.I. Wright, J.A. Basinger, M.M. Nowell, Angular precision of automated electron backscatter diffraction measurements, *Mater. Sci. Forum* **702-703** (2011) 548–553.

- [26] A. Morawiec, E. Bouzy, On the reliability of fully automatic indexing of electron diffraction patterns obtained in a transmission electron microscope, *J. Appl. Cryst.* **39** (2006) 101–103.
- [27] P.E. Champness, *Electron Diffraction in the Transmission Electron Microscope*, BIOS Scientific Publishers, Oxford, 2001.
- [28] T. Karthikeyan, M.K. Dash, S. Saroja, M. Vijayalakshmi, Evaluation of misindexing of EBSD patterns in a ferritic steel, *J. Microsc.* **249** (2013) 26–35.
- [29] N. Shigematsu, D. Prior, J. Wheeler, First combined electron backscatter diffraction and transmission electron microscopy study of grain boundary structure of deformed quartzite, *J. Microsc.* **224** (2006) 306–321.

## Captions

Table 1: Implementations of TEM-based automatic orientation mapping including distinct variants. Symbols in the second column indicate method of pattern acquisition and method of indexing: **A** – dark field imaging, **B** – stepwise scanning, **a** – grid search, **b** – detection of reflections.

Table 2: Experimentally estimated precision of orientation and misorientation determination for typical mapping conditions. The precisions are given as two standard deviations, i.e. with the confidence of 95%. Data are listed with one decimal digit (in degrees) after rounding up. The numbers in parentheses are for the rotations about axes perpendicular to 'z'. The italicized numbers indicated by arrows were obtained using the relationship between the standard deviations for orientations and misorientations (eq. 1).

Figure 1: An example raw large angle convergent-beam electron diffraction pattern from a thin specimen (*a*) and the same pattern with Kikuchi lines enhanced by background subtraction (*b*).

Figure 2: (*a*) Illustration of precision in Kikuchi-based orientation determination. The patterns with  $\xi \approx 17^\circ$  originated from a Ti- $\alpha$  specimen. Boxes represent deviations from the average orientations. Stars represent deviations of automatically determined orientations from the average orientations. The ellipses are drawn at two standard deviations from the mean. (*b*) Precision of orientation determination from Kikuchi patterns of Si recorded with larger camera length (acceptance angle of  $2.3^\circ$ ) [22]. Reproduced with permission of the International Union of Crystallography (<http://journals.iucr.org/>). All angles are given in degrees.

Figure 3: Illustration of accuracy in determination of misorientations between coherent twins using Kikuchi patterns; deviations from the exact  $\Sigma 3$  misorientation. The ellipses are drawn at two standard deviations from the mean.

Figure 4: (*a*) One of the diffraction patterns of Al containing both spot and Kikuchi components used in the test of precision in orientation determination by spot patterns. (*b*) Cumulative distributions of deviations of spot-based orientations from Kikuchi-based orientations for four different sets of spot pattern templates. The value of, say 90, for  $1.5^\circ$  means that 90% of results were within  $1.5^\circ$  angular distance from the Kikuchi-based orientations. (*c*) Deviations [in degrees] of orientations determined using spot patterns ( $5975 \times 600$  templates) from those obtained via Kikuchi diffraction. The large ellipses represent two

standard deviations from the mean (marked by crosses) for the displayed points. The small ellipses represent two standard deviations for the (Kikuchi) data of Fig. 2a.

Figure 5: Microstructure images of the investigated Al specimen at two tilts ( $7^\circ$  difference). Dashed lines mark the area of orientation mapping.

Figure 6: Example near- $\langle 215 \rangle$  diffraction patterns from the set used for creating maps shown in Fig. 7. (a) Processed Kikuchi pattern. (b) Spot pattern. (c) The same pattern as in (b) after enhancement of Kikuchi lines.

Figure 7: Maps of cell structure in Al ( $2 \times 2 \mu\text{m}^2$ ). Drawn boundaries correspond to  $0.8^\circ$  misorientation angles. (a) Map based on Kikuchi patterns. (b) Map based on spot patterns ( $976 \times 240$  templates followed by refinement). (c) Map based on Kikuchi patterns retrieved from spot patterns. (d) Inverse pole figure (in stereographic projection) illustrating the spread of orientations in map (a); the part containing most poles is magnified in the circle. No clean-up in (a) and (b). Spikes and pixels without solutions were removed from (c), but they are shown in Fig. 9a.

Figure 8: Example misorientation profiles along lines marked in the lower left inset (i.e., through bands and inside a band) for the Kikuchi-based map (Fig. 7a). The right inset shows analogous profiles obtained from the map based on spot patterns (Fig. 7b).

Figure 9: (a) Map of angular distances between orientations shown in Figs. 7 (b) and (c). The green pixels correspond to pixels with distances exceeding  $5^\circ$  (mainly spikes and pixels without solutions of Fig. 7(c)). (b) Cumulative distribution of deviations of spot-based orientations from Kikuchi-based orientations. The value of, say 80, for  $1^\circ$  means that 80% of spot based results were within  $1^\circ$  angular distance from the Kikuchi-based orientations.

Figure 10: Diffraction patterns of ferrite for the accelerating voltage of 200kV. (a) Simulated  $\langle 111 \rangle$  spot pattern for the acceptance angle of  $9^\circ$ . Reflections with kinematic intensities exceeding  $\sim 0.02$  of the most intense (110) reflection are shown. The pattern has six-fold symmetry and corresponds to two non-equivalent ( $\Sigma 3$ -related) orientations. (b) Simulated wide angle  $\langle 111 \rangle$  Kikuchi pattern and two near- $\langle 111 \rangle$  experimental patterns. The arc in one of the experimental patterns marks  $\xi \approx 17^\circ$ . If only black reflections with kinematic intensities exceeding  $\sim 0.05$  are detectable, none of the two experimental patterns gives a unique orientation. The left pattern gives a unique orientation if also red reflections with intensities exceeding 0.01 are detected.

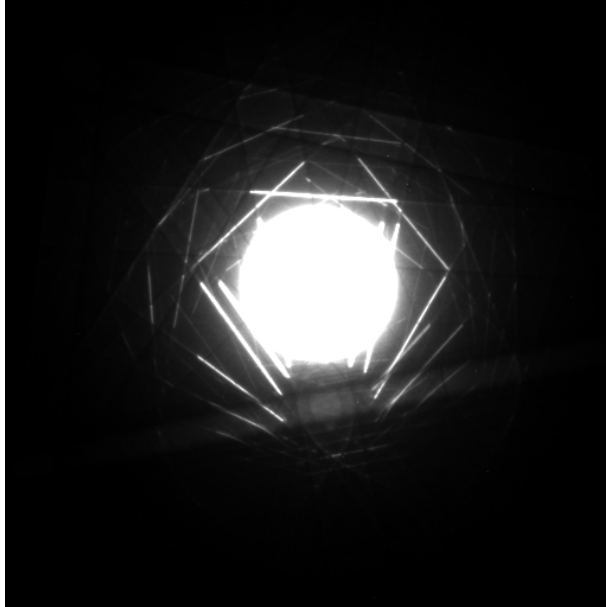
Description	Acqn & Indx	Source and year
• conical dark field scanning	A & <b>b</b> , spot	Wright and Dingley, 1998 [7,10]
— template matching	A & <b>a</b> , spot	Wu and Zaefferer, 2009 [12]
— 3D variant	A & <b>b</b> , spot	Liu et al., 2011 [13]
• nano-beam diffraction	B & <b>a</b> , spot	Rauch and Dupuy, 2005 [9]
— PED	B & <b>a</b> , spot	Rauch et al., 2008 [17]
— spot detection	B & <b>b</b> , spot	Kumar, 2013 [16]
• Kikuchi diffraction	B & <b>b</b> , Kikuchi	Morawiec et al., 2002 [18,19]

Table 1:

Precision – 95%				
	orientation, $2\sigma_o$		misorientation, $2\sigma_m$	
Spot, B & <b>a</b>	1.1°	→	1.5°	
Kikuchi, B & <b>b</b>	0.3° (0.1°)		0.4° (0.1°)	
EBSD	0.6°	←	0.8°	

Table 2:

*a*



*b*

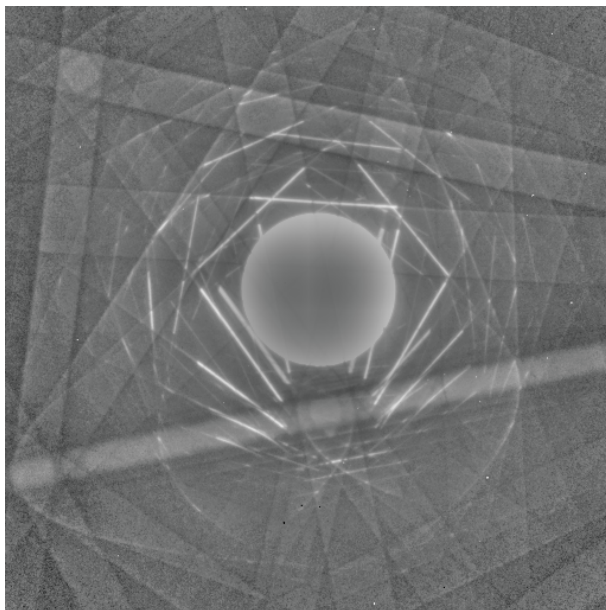


Figure 1:

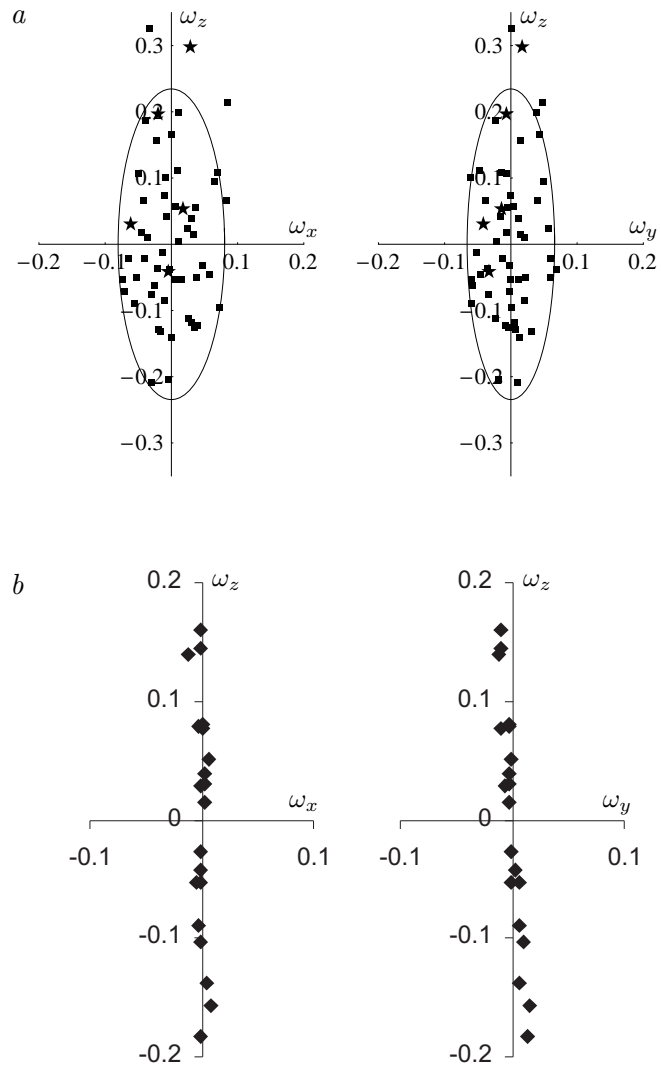


Figure 2:

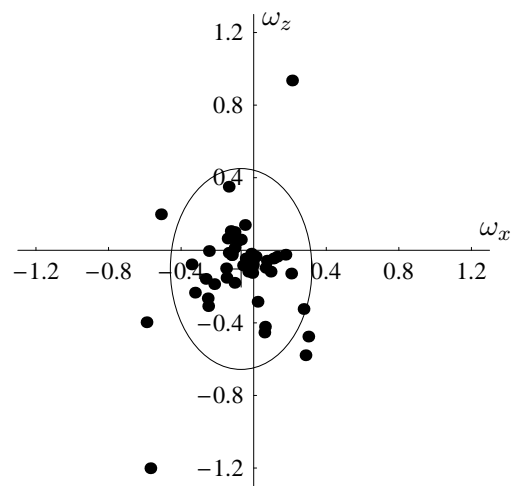
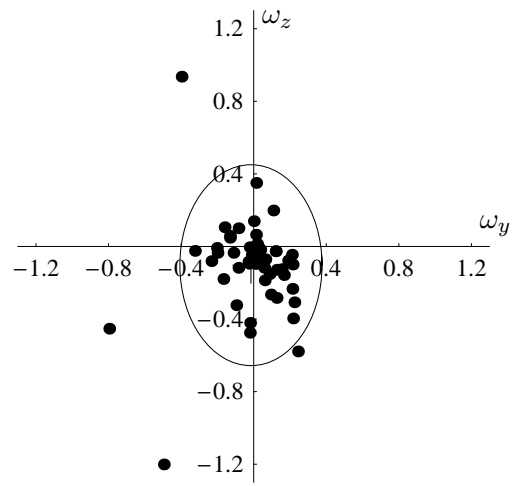
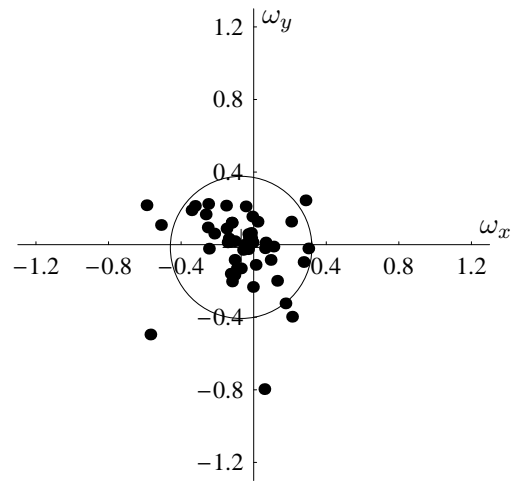


Figure 3:

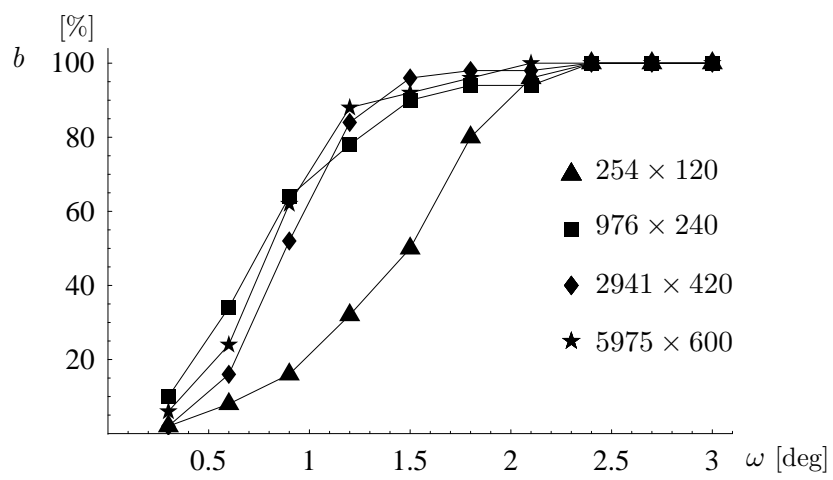
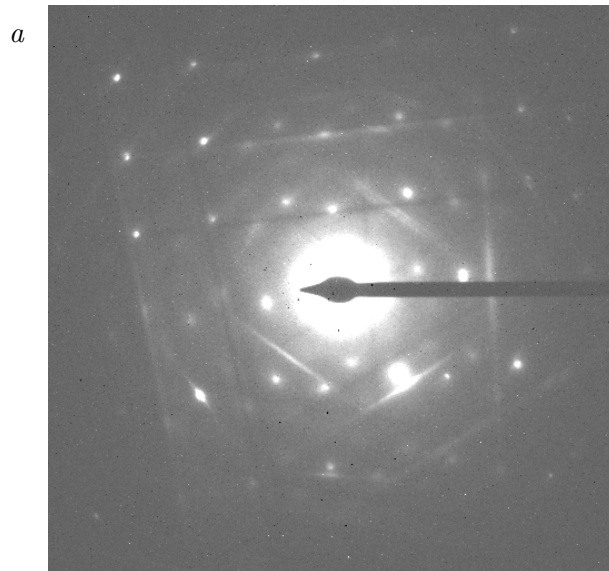


Figure 4:

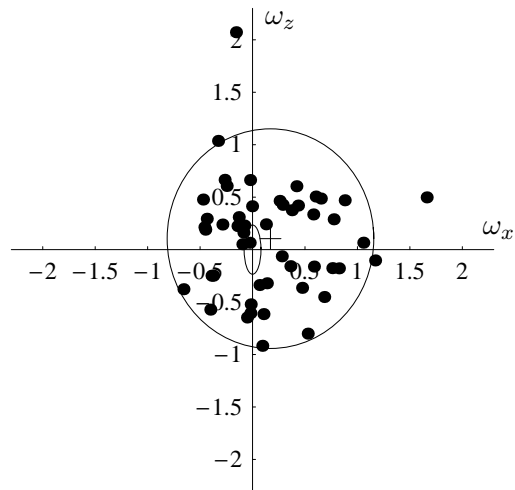
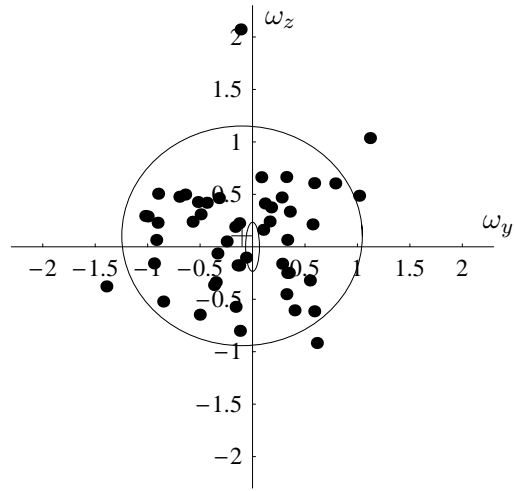
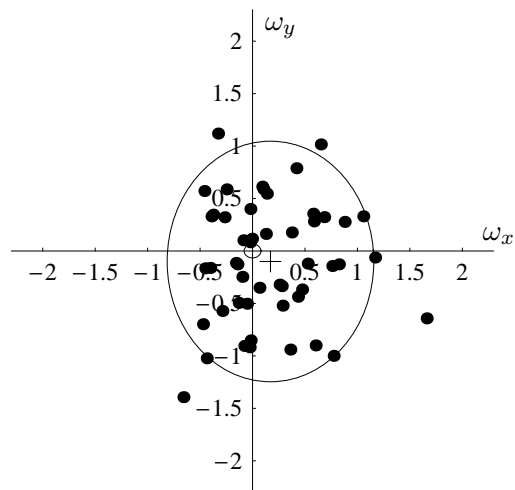


Figure 4c

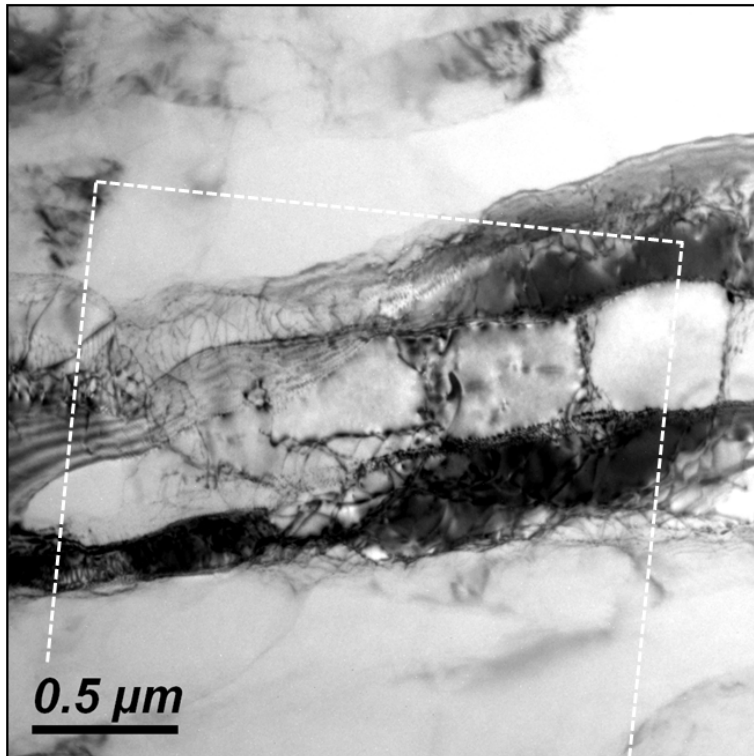
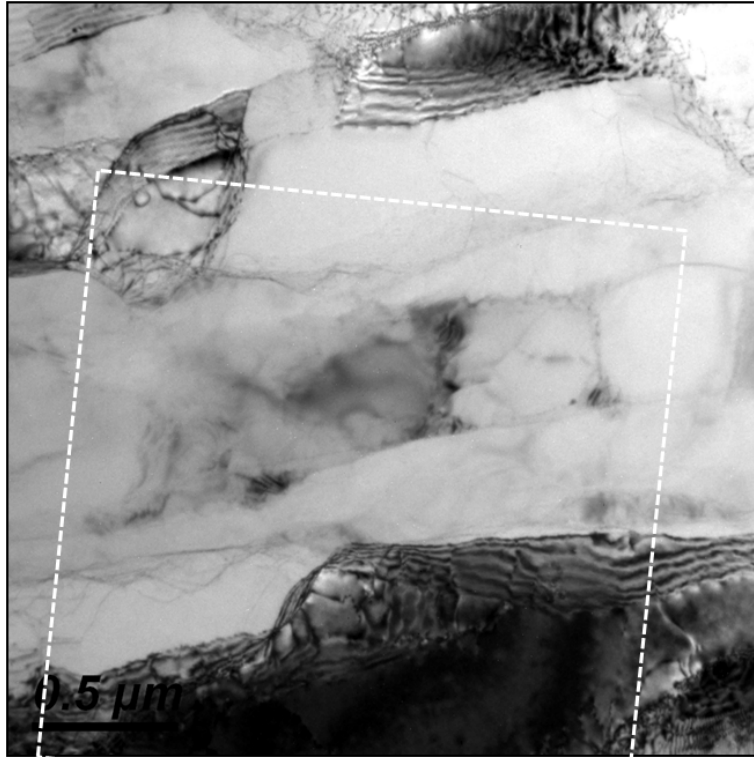
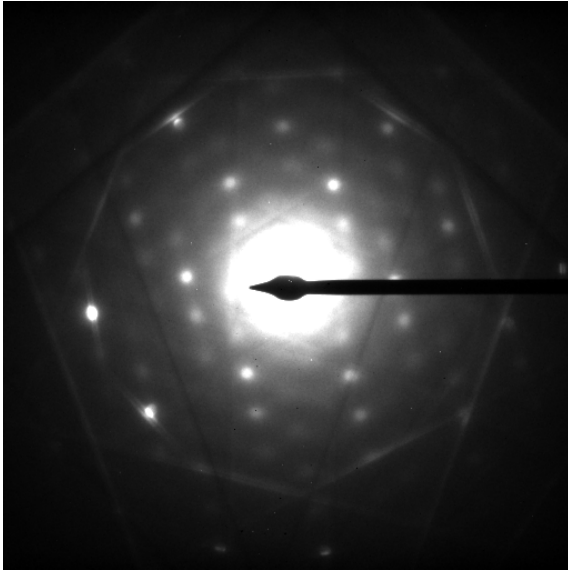
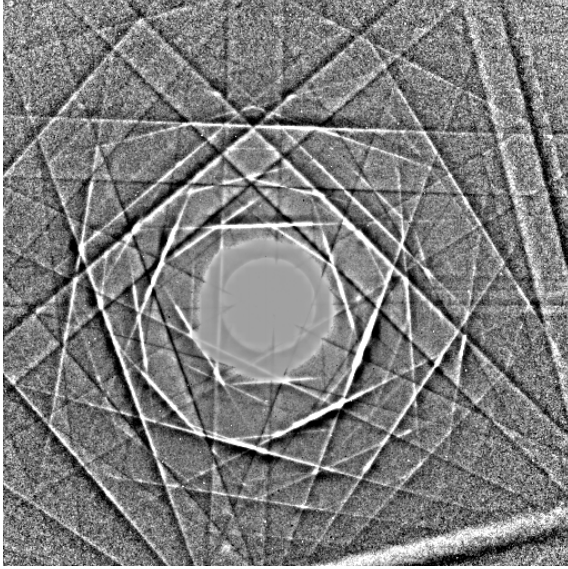
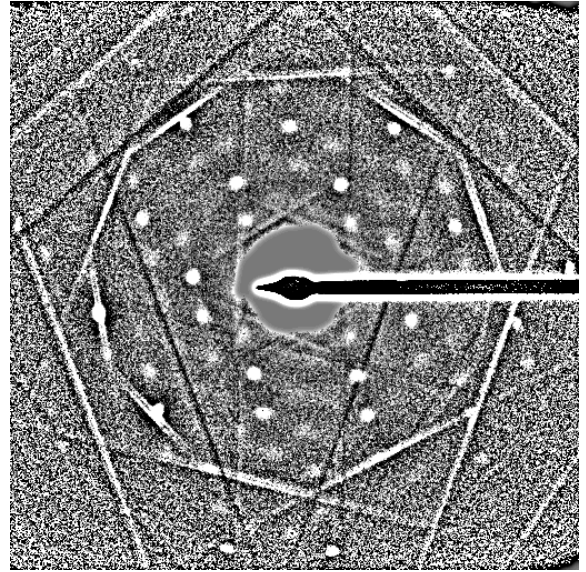


Figure 5:

*a*



*b*



*c*

Figure 6:

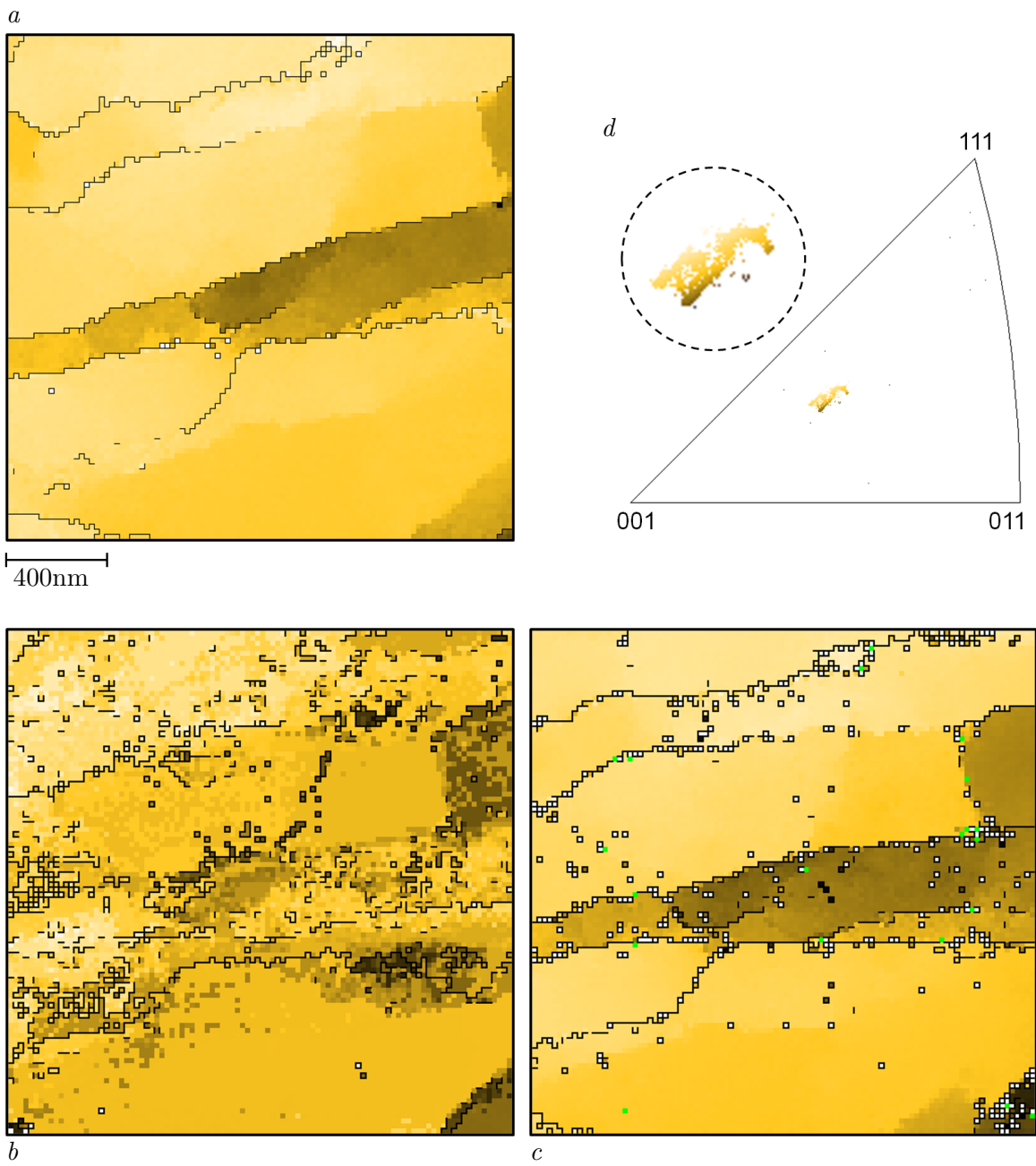


Figure 7:

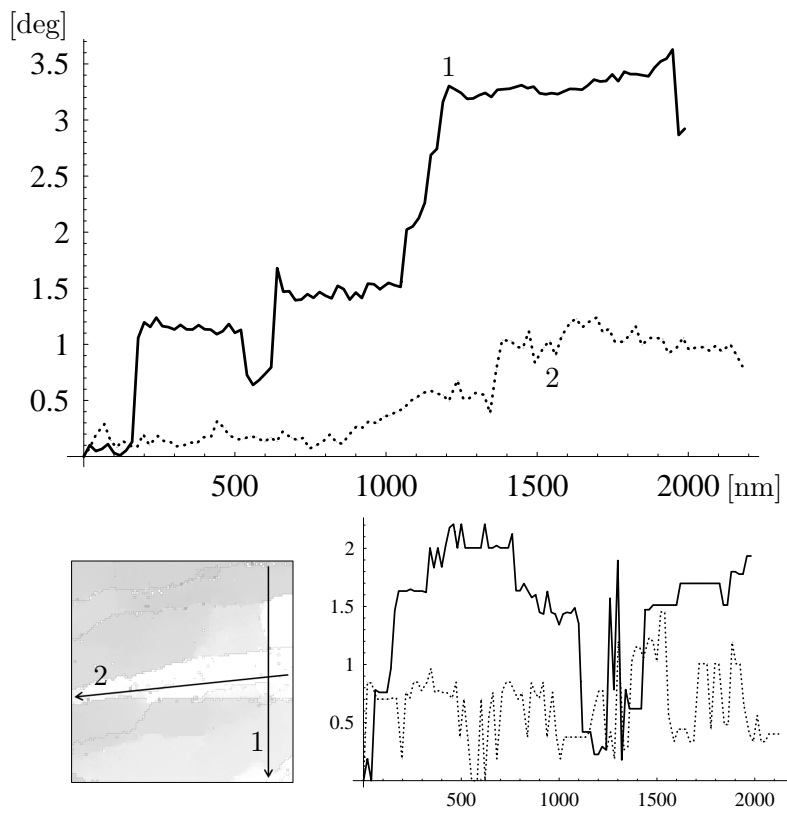


Figure 8:

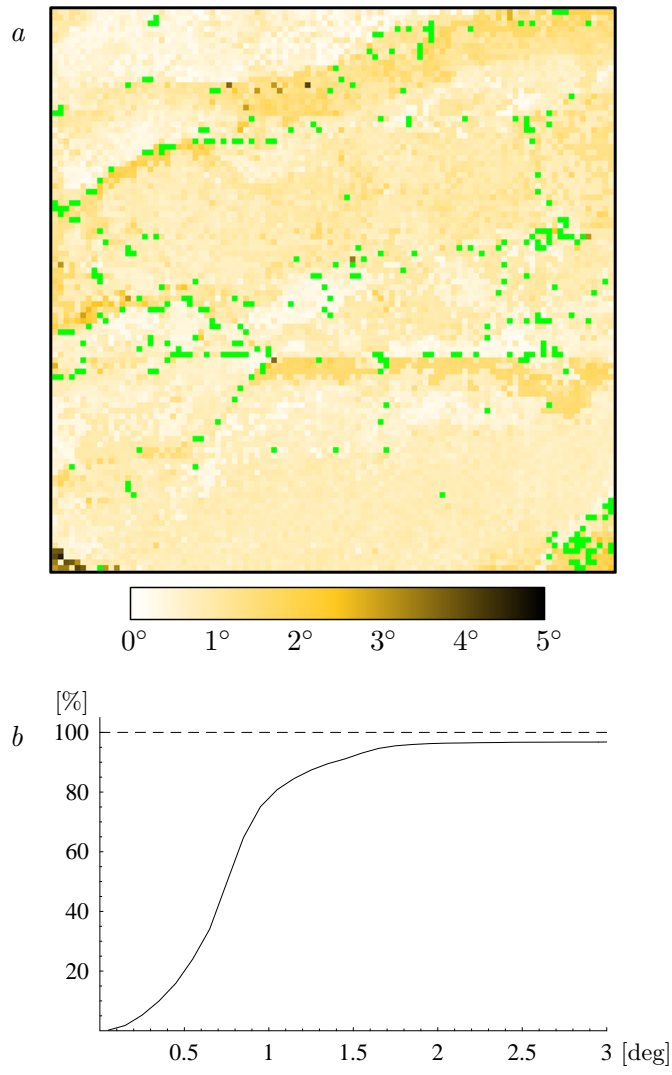


Figure 9:

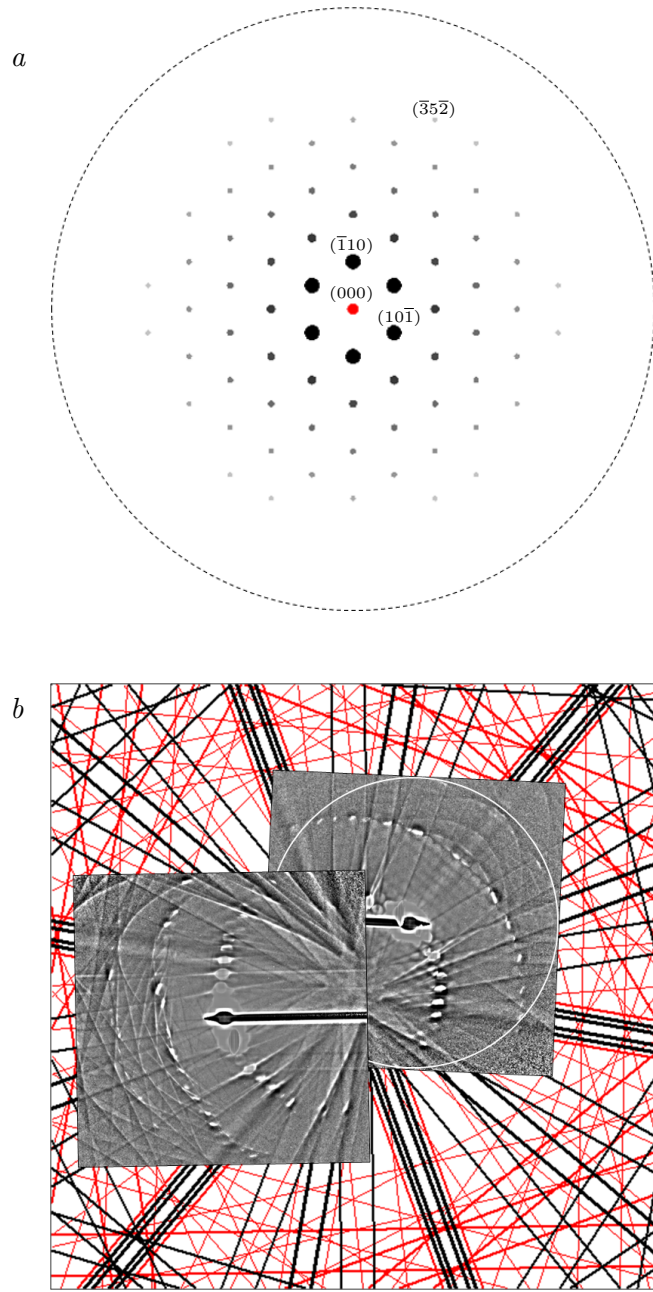


Figure 10: